Biomedical Signal Processing and Control 40 (2018) 252–262

Contents lists available at ScienceDirect

Biomedical Signal Processing and Control

journal homepage: www.elsevier.com/locate/bspc

Research Paper

Optimal selection of features using wavelet fractal descriptors and automatic correlation bias reduction for classifying skin lesions

Saptarshi Chatterjee*, Debangshu Dey, Sugata Munshi

Electrical Engineering Department, Jadavpur University, Kolkata-700032, India

ARTICLE INFO

Article history:
Received 15 May 2017
Received in revised form 7 September 2017
Accepted 30 September 2017
Available online 9 October 2017

Keywords:
Correlation bias reduction
Fractal descriptor
Melanoma
Recursive feature elimination
Support vector machine
Wavelet packet decomposition

ABSTRACT

The non-invasive computerized image analysis techniques have a great impact on accurate and uniform evaluation of skin abnormalities. The paper reports a method for the texture and morphological feature extraction from skin lesion images to differentiate common melanoma from benign nevi. In this work, a 2D wavelet packet decomposition (WPD) based fractal texture analysis has been proposed to extract the irregular texture pattern of the skin lesion area. On the whole 6214 features have been extracted from each of the 4094 skin lesion images, by analyzing the textural pattern and morphological structure of the lesion area. For the identification of the most efficient feature set, an improved correlation bias reduction method has been introduced in combination with support vector machine recursive feature elimination (SVM-RFE). An automatic selection of correlation threshold value has been introduced in this proposed work to eliminate the correlation bias problem associated with SVM-RFE algorithm. With these selected features, the support vector machine (SVM) classifier with radial basis function is found to achieve the classification performance of 97.63% sensitivity, 100% specificity and 98.28% identification accuracy. The results show that the scheme presented in this paper surpasses the performance of the other state-of-the art techniques for the differentiation of melanoma from other skin abnormalities.

1. Introduction

Among the most frequent types of cancer, the incidence of skin cancer has increased dramatically over the last few decades. Computer aided diagnostic (CAD) system has played an important role in the field of medical diagnosis and further decision making for early detection and prevention of skin cancers. Melanoma or malignant melanoma, usually developed from pigment-containing cells (melanocytes), has been contemplated as most deadly variety among all types of skin cancers [1]. In the detection of melanoma, a gold standard non-invasive imaging technique known as dermoscopy has been widely accepted by the medical personnel for in-depth visualization of morphological structures, forms and colors that cannot be assessed by visual inspections only [2,3]. To quantify the dermoscopic findings and effectively distinguish melanoma from other skin diseases, different algorithms have been extensively used by expert dermatologists. Development and utilization of some powerful methods for the identification of geometrical, structural, texture and color properties of skin lesions, such as ABCD rule of dermoscopy [4], 7-point checklist [5], Menzies method [6] etc. have improved the diagnostic accuracy in comparison with the simple visual inspection, by 5–30%. Despite the introduction of dermoscopy, the melanoma diagnostic accuracy is still not greater than about 85% for experienced dermatologist [7]. Examples of dermoscopic images for atypical nevus and common melanocytic skin lesion have been shown in Fig. 1.

To increase the accuracy of diagnosis of skin diseases by providing a second opinion to the expert dermatologists, a number of methodical approaches have been proposed in the literature using image processing techniques in the area of computer-aided diagnosis. Aiming at classification of skin diseases, most of the CAD systems consist of four steps: image segmentation, border detection, feature extraction and finally the feature selection followed by image classification.

The standard approach for morphological feature extraction and structural analysis is to extract the lesions area from the skin lesion images using efficient segmentation method. The wide variety of lesions in terms of structural shape and size with irregular nature makes it very difficult to segment and identify the border irregularity from dermoscopic images. To address this problem, numerous

* Corresponding author.
E-mail address: saptarshichatterjee2009@gmail.com (S. Chatterjee).

https://doi.org/10.1016/j.bspc.2017.09.028
1746-8094/

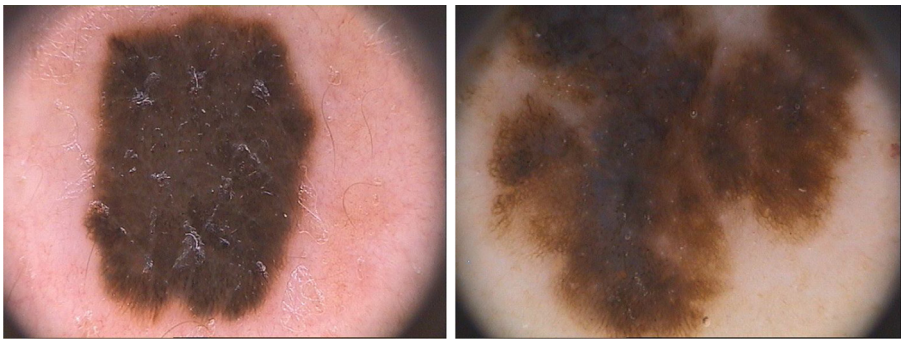

Fig. 1. Typical examples of dermoscopic images (a) atypical nevus and (b) melanoma.

segmentation and border detection techniques have been proposed in the literature [8–10]. In the work presented in this paper, our recently proposed mathematical morphology based segmentation and border detection technique [11], has been applied for the accurate identification of skin lesion area and the pixel locations along the lesion border.

For the accurate characterization of skin abnormalities, the use of feature extraction techniques for the quantification of visual interpretation of dermatologists, followed by segmentation and border detection plays an important role. In the literature, different methods for the extraction of features related to shape, border, texture and color from dermoscopic images have been reported.

Differentiation of melanoma from dysplastic nevi has been done with a sensitivity of 98% and specificity of 70% by Rastgoo et al. [12] using different shape, texture and color related feature extraction techniques, from global and local regions of dermoscopic images.

Shimizu et al. [13] have proposed a layered model for the classification of four different types of skin diseases and a flat model as a classification performance baseline. Different statistical color features with geometrical distribution of the color along the lesion area and GLCM based texture features have been extracted from each of the images.

In [14], Maglogiannis et al. have achieved a classification accuracy of 90.38% by extracting globules and dot related morphological features in dermoscopic images. Among all of the demarcating features of melanoma, such as asymmetry, border irregularity, atypical structures and colors, the textural pattern is the most subjective in nature. It is very difficult to characterize the textural pattern of the skin lesion by visual inspection only.

Garnavi et al. [15] have proposed a wavelet based texture analysis technique and boundary-series analysis for the diagnosis of melanoma with an accuracy of 91.26%. In literature, several other significant feature extraction and classification algorithms have been proposed in literature for the characterization of different biomedical images, [16–21].

In the work reported here, a systematic strategy has been formulated for the extraction of morphological and texture features of skin lesions. A set of well-known and important morphological features have been extracted from each of the segmented images. For the estimation of the irregular nature of the lesion border, wavelet based fractal dimension measurement technique has been proposed.

For the extraction of texture related features, most of the works employ different state-of-the-art techniques involving Gray-level Co-occurrence Matrices (GLCM) [22], Gabor- wavelets [23], Local Binary Pattern [24] etc, to describe the intensity distribution in the region of interest. However a more thorough approach is necessary for the estimation of the textural pattern of the skin lesion area. Here, we focus on the fractal descriptor approach based on wavelet packet decomposition to compute the fractality of the skin texture in the wavelet space. Fractal descriptor expresses the complexity at different wavelet decomposed levels within the texture and gives a detailed representation of the analyzed images.

From a wide range of extracted features, selection of the most demarcating features between different classes ensures the accurate classification of the images. Some of the important reported feature selection methods in this domain include genetic algorithm [25], principal component analysis [26], etc. In the present work, prior to the classification, recursive feature elimination (RFE) method combined with correlation bias reduction (CBR) technique [27], has been used for the selection of most appropriate and informative set of features. After the efficient feature selection step, melanoma and dysplastic nevi have been classified from the dermoscopic image datasets.

Hence, the contributions of the present work can be summarized as follows.

- A wavelet fractal descriptor has been introduced for the characterization of textural pattern of the skin lesion area. The original skin lesion images have been decomposed into different levels using wavelet packet decomposition technique and a fractal descriptor has been used for the extraction of textural distribution on the skin lesion area.
- For the border irregularity measurement, a border series has been obtained after calculating the pixel distance from central location to each of the border pixel locations. The border series, as a 1-D signal has been decomposed using three level wavelet decomposition technique, and Higuchi and Katz fractal dimension have been calculated from each of decomposed signals for the estimation of border irregularity.
- A classification algorithm by deploying automatic selection of correlation threshold value for SVM-RFE with CBR feature selection technique has been introduced in this proposed work, which may be considered as another novelty of the work.

This research paper is organized as follows. A brief introduction on fractal geometry has been given in Section 2. The image segmentation and border detection technique have been briefed in Section 3. The proposed wavelet packet fractal texture analysis followed by the border irregularity measurement technique has been described in Sections 4 and 5 respectively. The feature selection method together with the classification technique has been discussed in Section 6 followed by the results and discussion in Section 7. Finally, the paper has been concluded along with the future scope of the work in Section 8.

2. Fractal geometry

Fractals describe objects having unusual and high degree of complex properties with irregular shapes. The fundamental con-

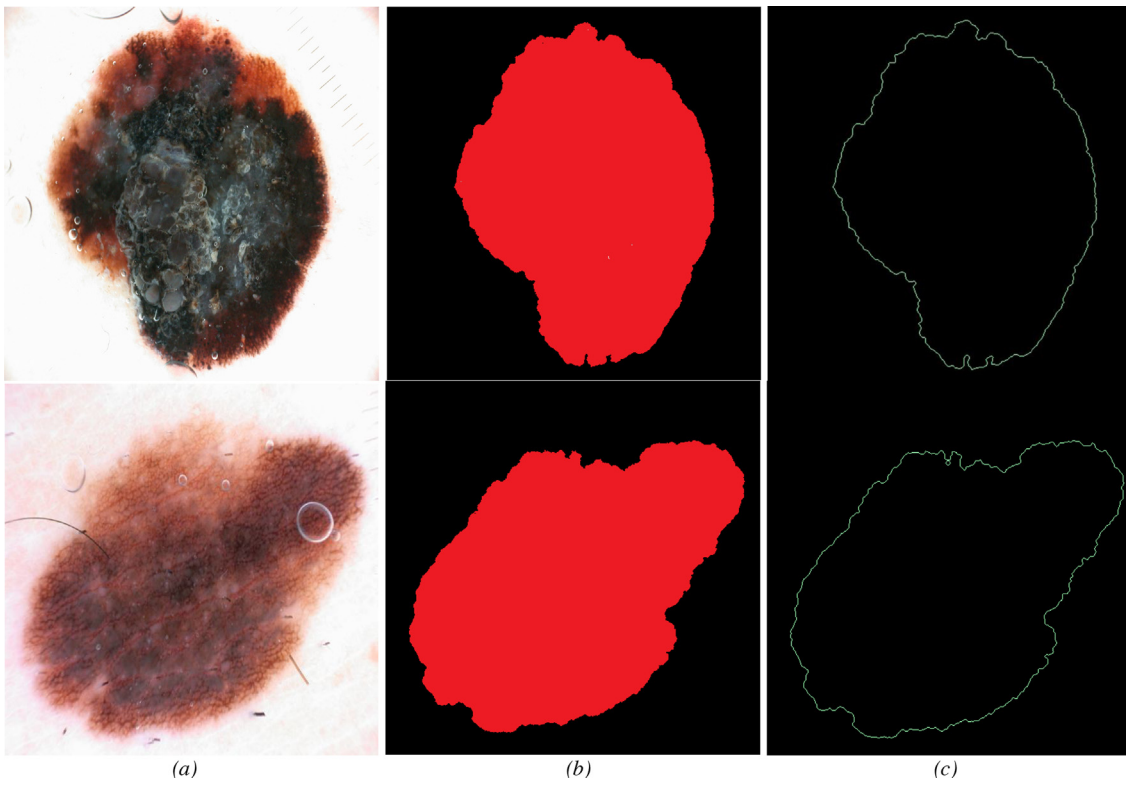

Fig. 2. (a) original color dermoscopic image, (b) segmented image and (c) border detected image of common melanoma and benign nevi respectively.

sideration of fractal geometry is the notion of dimension [28–31]. Dimension indicates how much space a set occupies close to each of its points. Among the wide variety of 'fractal dimensions', the definition of Hausdorff is the most important and convenient one. Hausdorff dimension is based on measures, which are relatively easy to manipulate [32]. Mathematically, the dimension D_H of a geometrical set F is calculated by the following expression:

$$D_H(F) = \inf_{d} \left\{ d \geq 0 | K_H^d(F) = 0 \right\} \tag{1}$$

where, $D_H(F)$ d-dimensional Hausdorff measure of F, defined by:

$$K_H^d(F) = \inf \left\{ \sum_{i=1}^{\infty} |X_i|^d : \left\{X_i\right\} is a\, r - cover \;\; of\, F \right\} \tag{2}$$

where $\left\{X_i\right\}$ is a finite collection of sets with diameter at most r ($r > 0$), that covers F.

An alternative and simpler form for the fractal dimension measurement of a complex object is given by,

$$\mathrm{D} = \lim_{l \to 0} \frac{\log(M)}{\log(l)} \tag{3}$$

Here, l is the size of the geometrical shape, which has to be used M number of times to cover the fractal object.

In [33], a general expression has been given for the development of simple and efficient algorithm for the computation of fractal dimension of any fractal-like object represented in discrete domain as

$$D \propto \frac{\log(n(\delta))}{\log(\delta)} \tag{4}$$

where n is a measure of self-similarity and δ is a scale parameter.

3. Segmentation and border detection

Image segmentation is a technique to segregate the region of interest from the entire image. Prior to the feature extraction and classification of skin diseases, the segmentation and the border detection are important. Most of the skin images are contaminated with noise and hair artifacts, and those have been removed using median filter and morphological bottom hat filter [34] in the preprocessing stage. The grey scale mathematical morphology has been used for the skin lesion segmentation with a circular kernel as a structuring element (SE) of eight pixel diameter. From the segmented image, some morphological features namely area, eccentricity, solidity, perimeter, equivalent diameter, rectangularity, major axis length, minor axis length, aspect ratio and elongation have been extracted.

For the border detection of the skin lesion area, the morphological gradient operation (subtraction of eroded image from the original image) with the circular kernel of two pixel diameter has been performed. This method helps to identify the single pixel border from the segmented image. The segmented and border detected image of malignant melanoma and benign nevi have been shown in Fig. 2.

4. Proposed wavelet packet fractal texture analysis

Among the wide variety of important features for the characterization of skin abnormalities, texture related features are the most subjective in nature. Understanding the visual texture plays an important role in computer aided diagnosis of skin diseases. As reported in the existing literatures, the texture analyses are performed either in spatial domain, or in frequency domain, or even using the combination of both. In the spatial domain, the texture features are extracted by means of some statistical measures of local texture patterns, whereas frequency domain analyses give some other essential characteristics of texture. To use the spa-

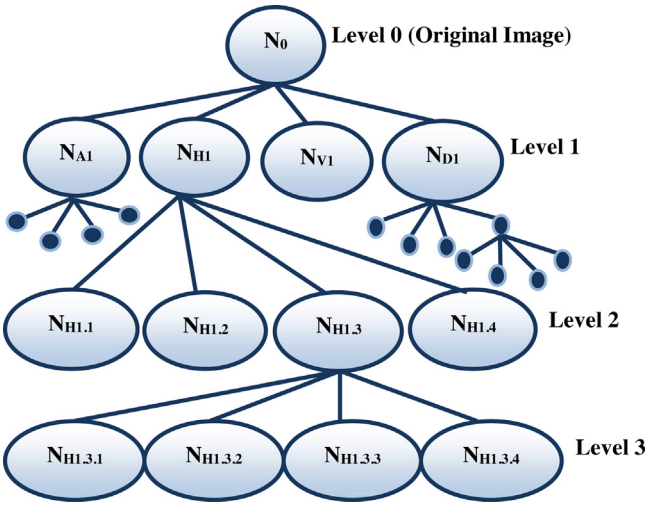

Fig. 3. Schematic representation of the wavelet packet decomposition technique.

tial and frequency domain information, some authors proposed time-frequency domain approach based on wavelet transform for the texture analysis. In the work reported here, a texture analysis technique that combines the wavelet-based representation of the dermoscopic images and fractal texture analysis method, to obtain detailed and robust texture information.

4.1. Wavelet packet decomposition

Wavelet transforms use windows of varying width and offer greater flexibility for the analysis of images by detecting image discontinuities and details using short, high-frequency bases, and coarse features using longer, low frequency bases [35]. The wavelets measure intensity variations for an image along different directions. Wavelet transform decomposes an image into four parts: an approximation component and three detailed components. The horizontal component measures variations along horizontal edges, the vertical component responds to variation along rows or vertical edges and the diagonal component is related to variations along the diagonals.

The wavelet packet decomposition (WPD), originally known as optimal sub-band tree structuring, offers more detailed description of scaling behavior into position, frequency and scale terms than the discrete wavelet transform by means of iteratively decomposing the image-detail components. This results in a more flexible multi-resolution analysis. In WPD, both the approximations and the detail components are further decomposed into four coefficients to create a complete binary tree. The parent node is decomposed into one approximate and three detail components. In the second stage each of all those previous coefficients are further decomposed in a similar manner into four coefficients to generate sixteen coefficients. This process is continued until no further decomposition is possible. As shown in Fig. 3, N_0 is the original image or parent node, and it has been decomposed into approximate and detail coefficients (horizontal, vertical and diagonal) denoted as N_{A1}, N_{H1}, N_{V1} and N_{D1} respectively, in level 1.Similarly at level 2, the horizontal component has been further decomposed as $N_{H1.1}$, $N_{H1.2}$, $N_{H1.3}$ and $N_{H1.4}$ and so on.

4.2. Wavelet fractal descriptor

The fractal dimension estimated according to Eq. (4) is a single real valued number that does not adequately represent the complexity of the object. The entire fractality curve can however serve as a powerful representative model of the region of interest. This is known as fractal descriptor of an object. The fractality values under different scales provide complete information of the distribution of image pixel intensity across the image region. This important information on visual or physical attributes of the image region of interest leads to more precise and robust methodology to describe complex nature of the object.

As discussed in [36], the wavelet packet transform gives a large number of wavelet coefficients denoted as D_j^i, where i is the scale and j is the translation component. The wavelet coefficients are sorted in descending order according to their discrete energy value as follows:

$$\overline{D} : \left\{ |D_1| \geq |D_2| \geq |D_3| \geq \cdots |D_m| \rangle 0 \right\} \tag{5}$$

Here, the zero valued components of the wavelet coefficient vector have been discarded since they are not significant for the power-law scaling, as described below.

The coefficient vector $\overline{D}$ is very large in size and most of its coefficients are contaminated by statistical noise. So, to consider the information containing coefficients, only the elements of the $\overline{D}$ vector at exponential intervals of $n = 1, 2, 4, 8, \ldots 2^{\log_2 m}$ have been considered, according to a power law relation in [30].

The resultant vector in descending order is given by,

$$D : \left\{ \overline{D}(1), \overline{D}(2), \overline{D}(4), \overline{D}(8), \cdots, \overline{D}(2^{\log_2 m}) \right\} \tag{6}$$

D scales with n according to a power law relation,

$$D \propto n^{\lambda_D}$$

The procedure described above can be used for the estimation of the fractal descriptor of an image containing fractal like objects, as this dimension is linearly related to λ_D. In [33,36], the authors used wavelet based fractal descriptor method for the analysis of different textural patterns and also for the computation of dimension of neuron shapes. Acceptable results have been demonstrated in literature for wavelet fractal descriptor method.

4.3. Wavelet packet fractal texture analysis

The skin lesion images have self-similar nature with a uniform intensity distribution in the normal skin region, whereas a noticeable intensity variations along the region of interest. This textural pattern makes the skin lesion image texture analysis more subjective in nature. The characteristics, color and pattern of skins of different people vary across the different regions of the world, and also according to the age. The lesion may occur in various locations of human body which have skins of different nature. As an example, the skin of human skull differs from the skins of other regions of human body. As we are interested only on the textural pattern of the lesion area, the texture analysis of the entire dermoscopic image may not lead to the extraction of proper textural information. To overcome this problem, the segmented image (the region of interest) has been masked with the original color dermoscopic image for the exclusion of the normal skin areas from the purview of textural analysis. The time-frequency analysis of two-dimensional images give more detailed information about the intensity distribution of the digital images. The texture analysis in spatial domain based on different statistical features is not sufficiently describing the large intensity variations in different image regions [33]. The fractal descriptor in wavelet domain provides sufficiently large chunk of information that help to deal with complex structures like skin lesions.

In this research work, the texture features have been extracted from the four color channels of red, green, blue and luminance [15] using wavelet based fractal texture analysis, where

$$lumi\,nance = (0.3 \times R) + (0.59 \times G) + (0.11 \times B) \tag{7}$$

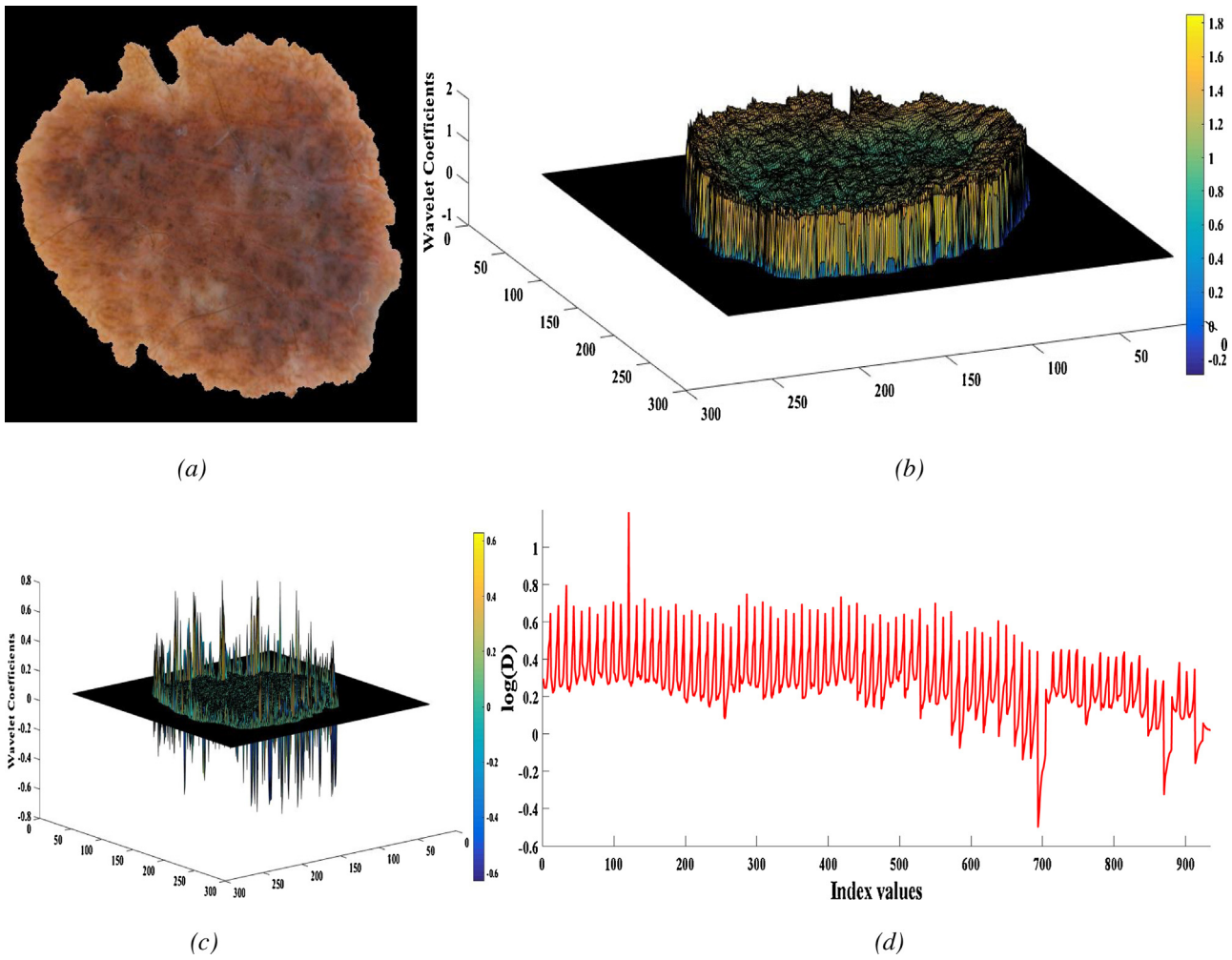

Fig. 4. (a) Original image masked with the segmented image, (b) low frequency component, (c) high frequency component after wavelet packet decomposition and (d) wavelet fractal descriptor of the R channel of the original color image for 3rd order Daubechies mother wavelet.

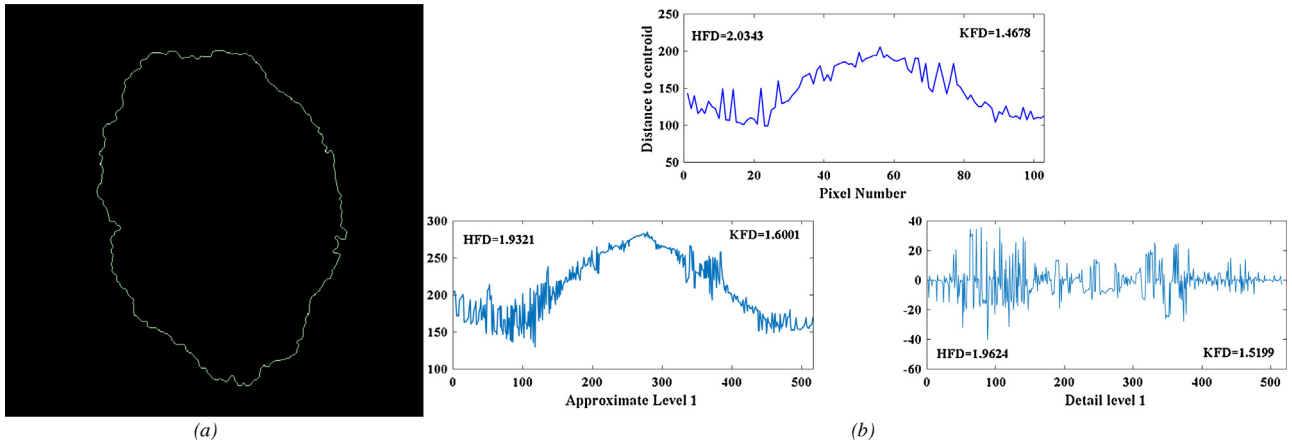

Fig. 5. (a) Border detected image of a benign nevi, (b) original border series (top) and approximate and detail representation at level 1 wavelet decomposition using Daubechies 3 mother wavelet (bottom).

The input image has been decomposed into different small and large coefficient values using three-level WPD technique. The three-level WPD decomposes the input image into overall 84 nodes (4 nodes in first level, 16 nodes in second level and 64 nodes in third level). From each of the nodes of the WPD along with the original image, some statistical features such as skewness, mean intensity, entropy, minimum intensity, maximum intensity, standard deviation, variance, and also the fractal descriptor have been extracted.

Instead of using the single valued fractal dimension, all the values in $\log(n(\delta))$ with reference to Eq. (4), have been considered to construct a fractal descriptor vector. To obtain the fractal descrip-

tor from each of the node of WPD, all the nonzero coefficient values have been sorted in descending order according to the power law as shown in Eq. (6). The resultant fractal descriptor vector has been obtained as,

$$D_f : \left\{ |\log(D(1))|,\ |\log(D(2))|,\ |\log(D(4))|,\ \cdots,\ |\log(D(\log_2 m))| \right\}$$

The combination of wavelet packet decomposition by employing classical Shannon entropy, and fractal descriptor characterizes the textural pattern of dermoscopic images by exploiting the complexity of the pixel distribution across the skin lesion area. The original lesion image along with its low frequency and high frequency components obtained using wavelet packet decomposition and fractal descriptor have been shown in Fig. 4. In Fig. 4(b) and (c) the reconstructed images from approximate and detail coefficients obtained using wavelet decomposition with 3rd order Daubechies mother wavelet, clearly exhibit the textural variations across the lesion area in time-frequency space. The reconstructed images also expose the intensity variations on the lesion area at different frequency regions which also have a self similar nature. The fractal descriptor as shown in Fig. 4(d) consists of all the fractality obtained from each of the 85 nodes of wavelet packet tree, including the original image. The complexity present in the lesion area at different frequency regions have been quantified using fractal descriptor.

5. Wavelet-fractal based border irregularity measurement

The irregular nature of the skin lesion is a very important and distinguishable feature for the proper identification of skin abnormalities. In the literature, various methodologies can be found for the quantification of border irregularity of the skin lesion in dermoscopic images by means of measuring the distance of the border points from the center pixel location of the segmented image. Inspired by the work on boundary-series features by Garnavi et al. [15] a fractal based border irregularity measurement technique in wavelet domain has been reported in this work. In this study, the distance between the center pixel location and each of the border pixel location (starting from an arbitrary border pixel location) has been calculated following the equation,

$$d_i = \sqrt{(x_i - x)^2 + (y_i - y)^2} \tag{8}$$

where d_i is the measured distance, (x_i, y_i) and (x, y) are the border pixel location and the center pixel location respectively. A border series has been obtained by constructing a finite length data as the pixel indices considered along the x-axis and the measured distance along the y-axis. The obtained border series has been decomposed into approximate and detail components via the application of three-level wavelet packet transform. From this three-level pyramid structured wavelet transforms, three pairs of approximate and detail components have been obtained. On the whole seven border series have been obtained by reconstructing all the decomposed coefficients, along with the original border series. In Fig. 5 the original border series of a lesion border image has been shown along with the approximate and details representation of first level wavelet decomposition using 3rd order Daubachies mother wavelet. Each of the obtained border series has been analyzed by means of extracting some histogram features namely mean, variance, skewness, kurtosis, energy and entropy. Other than the statistical features, the irregular nature of each of the obtained border series has been quantified by measuring Higuchi fractal dimension (HFD) and Katz fractal dimension (KFD).

A computationally very fast algorithm for the direct estimation of the fractal dimension without estimation of the strange attractor has been proposed by Higuchi [37]. For a given signal $S(n)$, l new time series $S(n)_m^l$ are constructed as,

$$S(n)_m^l = \left\{ s(m),\ s(m+p),\ \cdots,\ s(m + \lfloor \frac{N-m}{l} \rfloor . l) \right\} \tag{9}$$

where, $m = 1,2,\ldots,l$. Here the initial time and the time interval have been indicated by m and l respectively. The average length of m curves for each curve $S(n)$ has been obtained by:

$$L_{avg} = \frac{1}{l} \sum_{m=1}^{l} \left[\left(\sum_{i=1}^{\lfloor \frac{N-m}{l} \rfloor} |x(m+il) - x(m + (i-p)_p)| \right) . \frac{N-1}{\lfloor \frac{N-m}{l} \rfloor p} \right] \tag{10}$$

where, $N-1/\lfloor \frac{N-m}{l} \rfloor$ is a normalization factor. From the curve of $\log(L_{avg}(l))$ versus $\log(1/l)$, the slope of the least square linear best fit has been estimated as Higuchi's fractal dimension.

Katz [38] proposed another methodological approach for the fractal dimension measurement of the time series waveform. The fractal dimension of a curve can be estimated in accordance with Eq. (3), where M can be considered as the total length or sum of the Euclidean distances between successive points and l as the diameter of the curve, considered as the maximum of distances between the first sample and all consequent samples in the time series. Katz proposed a normalization method for l and M by the length of the average step or average distance between successive points, s, defined as $s = M$, where n is the number of steps in the curve. The Eq. (3) has been modified as,

$$D = \frac{\log(M/s)}{\log(l/s)} = \frac{\log(n)}{\log(l/M) + \log(n)} \tag{11}$$

Eq. (11) summarizes the Katz's methodology for fractal dimension measurement of a waveform.

The above mentioned fractal dimension estimation technique quantify the anomalous nature along the border of the skin lesion area.

6. Feature selection and classification

6.1. Feature selection

Prior to classification, the feature selection method is a very important step that helps to identify, the most appropriate and distinguishable features demarcating the target classes from the large number of features. An efficient feature selection algorithm not only increases the classification accuracy but also reduces the computation burden by reducing the data size. Among the several feature selection algorithms proposed in the literatures, the recursive feature elimination (RFE) method combined with nonlinear SVM has recently been introduced and has been found to be effective in various applications. RFE is a weight-based backward elimination or selection algorithm introduced by Guyon et al. [39].

The essences of the RFE method are to train the SVM classifier model with all the features and subsequently identify those that cause least decrement of the margin between the target classes. In this reported work, SVM-RFE algorithm combined with a correlation bias reduction (CBR) method [27] has been used for feature selection. The CBR is introduced to eliminate the problems associated with SVM-RFE, when a large number of highly correlated data exist.

6.1.1. Nonlinear SVM-RFE

The SVM was introduced by Boser et al. and thoroughly examined by Vapnik [40]. The basic idea behind SVM is to develop a separating hyperplane which disparate samples of different classes with maximal distance between the hyperplane and the closest

training data points [41]. In the RFE algorithm, the SVM model has first been trained with the entire candidate feature set and all those features have subsequently been ranked according to the order of their estimated weight value. In each iteration, the feature having smallest ranking criterion has been identified and removed, since it has minimum effect on classification. The remaining features have been subjected to the next iteration. Thus, eliminating the features in a recursive manner, they have been sorted in a way such that the feature eliminated later has been assigned higher ranking. For a large feature set, the elimination and selection of features in recursive manner is very time consuming and also introduce correlation bias problem.

The linear SVM-RFE is more suitable feature selection method when the numbers of samples are very less in comparison with the several thousands of features to avoid overfitting. As the nonlinear SVM-RFE can fit the data with less bias so, it is expected to be outperformed the linear one for the larger sample size (more than 100).

Nonlinear SVM maps the entire features into a higher dimension space. For a given set of training samples $\{x_i, y_i\}$, $x_i \in R^d$, $y_i \in \{-1, 1\}$, $i = 1, 2, \ldots, n$ the nonlinear SVM contemplates to map the feature set into a higher dimensional space:

$$x \in R^d \mapsto \varphi(x) \in R^h \tag{12}$$

In the new higher dimension feature space the samples are expected to linearly separable. Thus the Lagrangian formulation of nonlinear SVM can be written as

$$L_D = \sum_{i=1}^{n} \alpha_i - \frac{1}{2} \sum_{i,j=1}^{n} \alpha_i \alpha_j y_i y_j \varphi(x_i) \cdot \varphi(x_j) \tag{13}$$

where α_i are the Lagrange multipliers. Here we can replace $\varphi(x_i) \cdot \varphi(x_j)$ with a kernel function $K(x_i, y_j)$ without the information regarding φ as the only form that $\varphi(x)$'s have been involved in the training algorithm is their inner product. Among several kernel functions, the radial basis function (RBF kernel) is the common choice, given as

$$K(x_i, y_j) = e^{-\frac{\|x_i - x_j\|^2}{2\sigma^2}} \tag{14}$$

$\|x_i - x_j\|^2$ may be considered as squared Euclidean distance between two feature vectors. The Eq. (14) can be simplified by replacing $\gamma = \frac{1}{2\sigma^2}$ as,

$$K(x_i, y_j) = e^{-\gamma \|x_i - y_j\|^2} \tag{15}$$

Since the form of φ is unknown, the weight vector cannot be obtained. The ranking criterion for a feature k can be written as:

$$J(k) = \frac{1}{2} \sum_{i,j=1}^{n} \alpha_i \alpha_j y_i y_j K(x_i, x_j) - \frac{1}{2} \sum_{i,j=1}^{n} \alpha_i \alpha_j y_i y_j K(x_i^{(-k)}, y_j^{(-k)}) \tag{16}$$

The notation $(-k)$ indicates the removed k^{th} feature. The feature with smallest J's will be recursively removed from the feature set in iteration of RFE.

6.1.2. Correlation bias reduction

In the classification of high – dimensional data containing groups of correlated features, the assessment of the appropriacy of the feature is of utmost importance. To achieve this, the model that gives priority to the retrieval of all predictive features, should be preferred. Toloşi *et. al* in [42], appraised that the features in the correlated feature groups received smaller weights due to the partaken responsibility in the classification models. These smaller weights will act against the undermining of the importance of those features that are highly relevant. The elimination of features because of the incorrect underestimation of their ranking criterion is known as "correlation bias". To reduce the correlation bias, the most acceptable strategy is to group the correlated features prior to the model fitting and identify the feature representative of each group which defines the importance of the original features. SVM-RFE feature selection method eliminates one feature in each iteration according to their ranking criterion. Thus, this method is not efficient for higher dimension features. To overcome this issue, a group of features are eliminated in one iteration. This may lead to the removal of a group of correlated as well as relevant features entirely. Introduction of the correlation bias reduction technique move back the representative feature from the eliminated features set to the surviving features set. In each iteration, the group representative feature has been selected as the feature with the highest ranking criterion (weight value). This technique monitors and corrects the wrongly estimated weight and rank of features due to correlation bias, without changing ranking criterion of the original feature set. In different feature selection algorithms including SVM-RFE, highly correlated features bring wrong estimations of the weight and rank of the features [27].

In the preliminary stage of the SVM-RFE with CBR feature selection algorithm, features have been eliminated recursively according to their ranking criterion. A predefined threshold value has been selected as the elimination threshold. When the number of features in the existing feature set is more than the predefined elimination threshold value, the RFE method will eliminate a batch of features in each iteration. After reaching at the predefined threshold value, a single feature with lowest ranking criterion will be eliminated in the remaining iterations. The purpose of the inclusion of correlation bias reduction algorithm with SVM-RFE method is to move the potentially useful features from eliminated features set to surviving features set. In order to identify highly correlated feature groups, two threshold values, correlation threshold and group threshold, have been selected. In the eliminated feature set, the bunch of features (more than group threshold value) having an absolute correlation coefficient higher than the predefined correlation threshold value are considered as a group. If none of the group members are present in the existing feature set, then the feature with highest ranking criterion has been moved to the existing feature set as the group representative. This operation has been continued for all features in the eliminated features set.

6.2. Automatic selection of correlation threshold value

Yan *et. al* [27] has elaborated how different classification accuracies have been obtained for various settings of correlation threshold value. The correlation threshold value helps to identify the correlated features group. For different correlation threshold values, the representative feature of a group may change. The effect of the selection of different group representative for different correlation threshold value is usually reflected in the correct classification accuracy. In this work, to eliminate the effect of the correlation threshold value on the classification accuracy, the said threshold value has been varied to yield more and more improved classification accuracy. A wide range of correlation value has been selected from 0.5 to 1. For each of the selected threshold value, the features have been ranked according to their weight value using SVM-RFE with CBR technique. After the feature selection step, the images have been classified using support vector machine classifier with radial basis function. The performance of classification has been evaluated by calculating some standard parameters like the sensitivity (SN), the specificity (SP) and the accuracy (ACC). The correlation threshold value which leads to the solution with the best classification accuracy has been considered as final.

The number of selected most pertinent features also has an important bearing on the improvement in classification perfor-

Table 1
First five selected features using SVM-RFE with CBR technique.

Mother Wavelet	First Feature	Second Feature	Third Feature	Fourth Feature	Fifth Feature
Daubechies-3	Tex: FD_H1.2_B	BI: HFD_D1.2	Text: Ent_B	Text: FD_V1.2.2_B	Morph: Minor_L
Symlet-7	Tex: FD_D1.1_B	Text: FD_V1.2.1_B	Text: FD_V1.2.2_B	Text: Mean_H1.2_G	Morph: Minor_L
Coiflet-2	Text: Var_H1.2.4_B	Morph: Minor_L	Text: FD_V1.2.2_B	Text: Mean_H1.2_G	Text: FD_D1.2.3_B

Tex: Texture Features; Morph: Morphological Features; FD: Fractal Descriptor; Ent: Entropy; Minor_L: Minor axis length; HFD: Higuchi Fractal Dimension; Mean: Mean Intensity; Var: Variance; B: Blue channel of RGB color image; G: Green channel of RGB color image. H: Horizontal Coefficients; V: Vertical Coefficients; D: Diagonal Coefficients.

mance. In the algorithm presented in this paper, the correlation threshold value has been selected by classifying the test images with various number of selected features, i.e. maintaining the number of selected features for classification as constant and varying the correlation threshold value from 0.5 to 1, at an increment of 0.05. After selecting the correlation threshold value for each of the selected number of important features, varied from a maximum value of fifty to a minimum feature length of twenty, the classification performance has been evaluated at each stage.

7. Results and discussions

7.1. Database description

The entire research work has been done on the 4094 skin lesion images of two different classes, namely common melanoma and benign nevi diseases. The skin lesion images have been collected from some widely acceptable image databases, namely International Dermoscopic Society [43], Dermoscopic Atlas [44], PH2 database [45] and ISIC: challenge 2017 database [46].

7.2. Parameter selection

In this reported work, the first important decision for the three level wavelet packet decomposition method is the selection of suitable wavelets. Here, three of the most popular wavelets, namely Daubechies, Symlets and Coiflets, have been selected as mother wavelet function. For the wavelet packet fractal texture analysis and wavelet-fractal border irregularity measurement, filter with shorter length such as Daubechies 1 to Daubechies 10, Symlet 2 to Symlet 8 and Coiflet 1 to Coiflet 5 have been considered. So, for the entire analysis, twenty two different wavelet filters have been chosen and for each of the mother wavelet, the texture and border irregularity features have been extracted and classification performance has been evaluated.

For the selection of important and distinguishable features between the two classes of skin lesion images using SVM-RFE with CBR technique, three guiding parameters have been chosen as the group threshold value, the correlation threshold value and the elimination threshold value. Among these three parameters, the correlation threshold value has been selected automatically according to the best classification accuracy. A larger group threshold value identifies fewer groups and hence eliminates some groups of correlated features too early [27]. As a result, the classification accuracy is also degraded. Keeping in mind the effect of the group threshold value on classification performance, the entire feature selection has been done with a predefined group threshold value as 1. The elimination threshold value has been selected by rigorous exercised as sixty features. When the number of existing features is more than sixty, then half of the existing features will be move to the eliminated feature set at each iteration. When the number of features becomes sixty, a single feature will be eliminated in each iteration.

7.3. Results

In this research work, by analyzing the morphological pattern, irregular nature and textural pattern of the skin lesion, 6214 features have been extracted from each of the skin lesion images, with each of the previously mentioned twenty two mother wavelet functions. Using the SVM-RFE with CBR feature selection algorithm, the features that are most conspicuous in revealing the demarcation between melanoma and dysplastic nevi, have been selected according to their ranking criterion. Selecting the first 20, 30, 40 and 50 features at each stage the images have been classified using SVM classifier with RBF kernel using ten-fold cross validation method. The classification performance has been evaluated by calculating the sensitivity (SN), the specificity (SP) and the accuracy (ACC) during the classification stage.

7.4. Discussion

In this reported work the performance of the classification of common melanoma and benign nevi has been assessed for each of the selected mother wavelet. The classification performance has been evaluated by calculating sensitivity, specificity and accuracy for Daubechies, Symlet and Coiflet wavelet families, for different number of selected features. Prior to the classification, SVM-RFE with CBR feature selection algorithm has been used to rank the features according to their weight values and the images have been classified for first 20, 30, 40 and 50 selected features set. The entire exercise has been carried out by different features sets, selected using varying correlation threshold values from 0.5 to 1. At maximum correlation i.e. 1, the feature selection has been done using SVM-RFE, without introducing the CBR technique. In the entire work, very good and consistent correct identification accuracy has been achieved for most of the classifiers with a minimum accuracy of 85.05% for Daubechies-6 wavelet function with first 50 features. From the computations carried out, it has been found that better classification performance has been obtained for the lower order wavelet functions. With an efficient feature selection method, it is expected to classify the images with acceptable performance metrics using lesser number of features. In this proposed work the classification performance with first 30 features have been considered as the performance baseline. A minimum correct classification accuracy as 91.18% for 1st order and 3rd order Coiflet mother wavelet and maximum accuracy as 98.28% for 3rd order Daubechies wavelet have been achieved by considering first 30 selected features. For Daubechies wavelet family the maximum sensitivity, specificity and accuracy values have been achieved as 97.63%, 100% and 98.28% respectively with 3rd order mother wavelet. The highest sensitivity, specificity and correct classification accuracy have been achieved as 97.62%, 100% and 98.25% respectively for Symlet wavelet family. Similarly 95.99% sensitivity, 99.08% specificity and 96.81% correct classification accuracy have been obtained for 2nd order Coiflet wavelet using first 30 selected features.

The first five important features for 3rd order Daubechies, 7th order Symlet and 2nd order Coiflet wavelet functions have been given in Table 1. From Table 1 it can be seen that the fractal descriptor and statistical features related to the texture, are the most

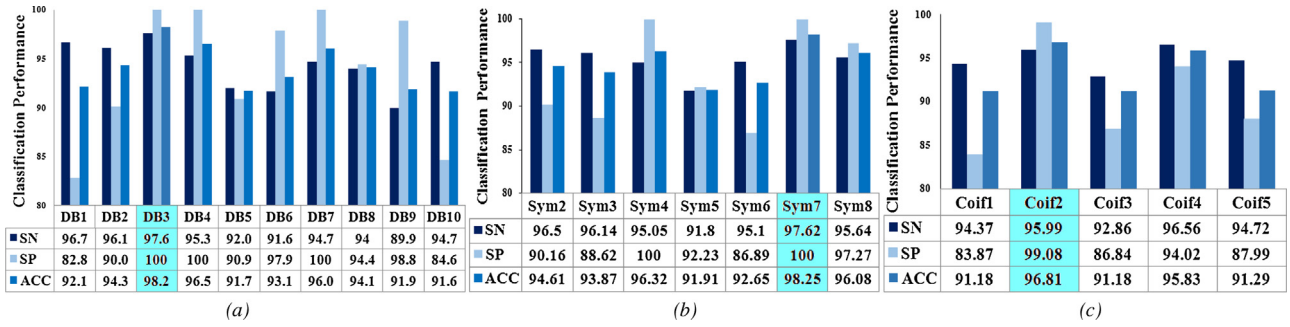

	DB1	DB2	DB3	DB4	DB5	DB6	DB7	DB8	DB9	DB10
SN	96.7	96.1	97.6	95.3	92.0	91.6	94.7	94	89.9	94.7
SP	82.8	90.0	100	100	90.9	97.9	100	94.4	98.8	84.6
ACC	92.1	94.3	98.2	96.5	91.7	93.1	96.0	94.1	91.9	91.6

	Sym2	Sym3	Sym4	Sym5	Sym6	Sym7	Sym8
SN	96.5	96.14	95.05	91.8	95.1	97.62	95.64
SP	90.16	88.62	100	92.23	86.89	100	97.27
ACC	94.61	93.87	96.32	91.91	92.65	98.25	96.08

	Coif1	Coif2	Coif3	Coif4	Coif5
SN	94.37	95.99	92.86	96.56	94.72
SP	83.87	99.08	86.84	94.02	87.99
ACC	91.18	96.81	91.18	95.83	91.29

Fig. 6. Classification performance of the proposed methodology using different wavelet families (a) Daubechies, (b) Symlets, (c) Coiflets for top 30 selected features using SVM-RFE with CBR technique.

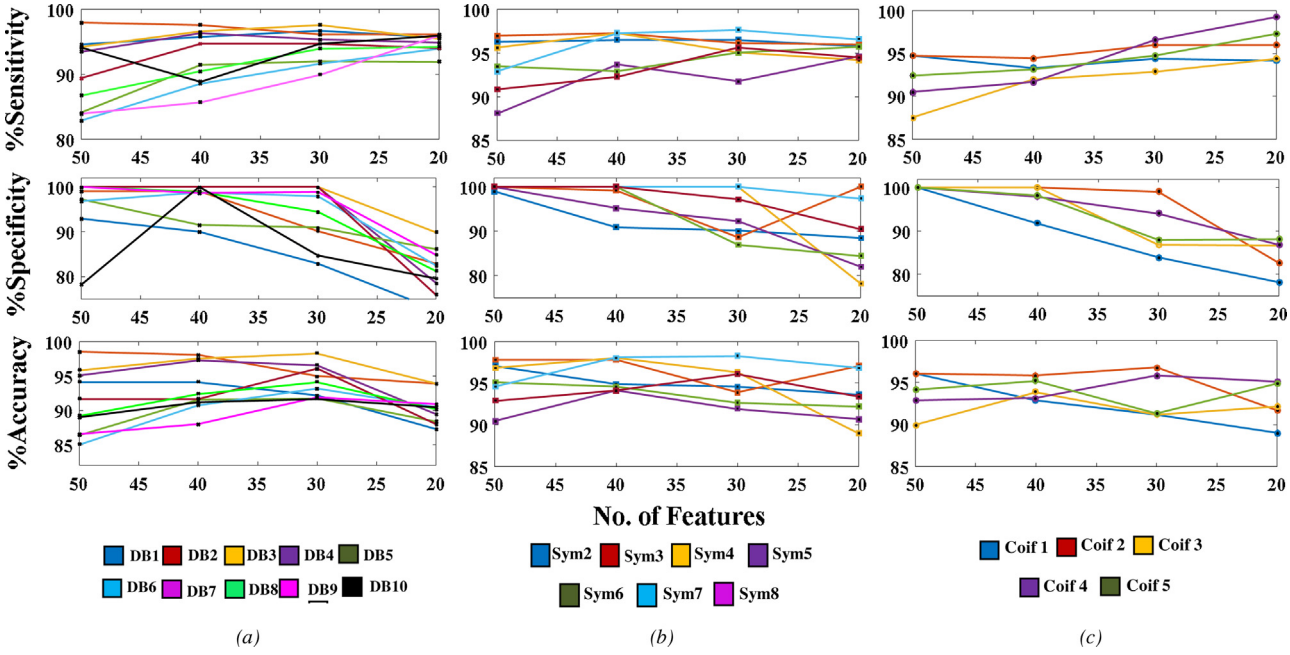

Fig. 7. Variations of the classification performance indices according to the number of selected features for (a) Daubechies, (b) Symlet and (c) Coiflet wavelet families.

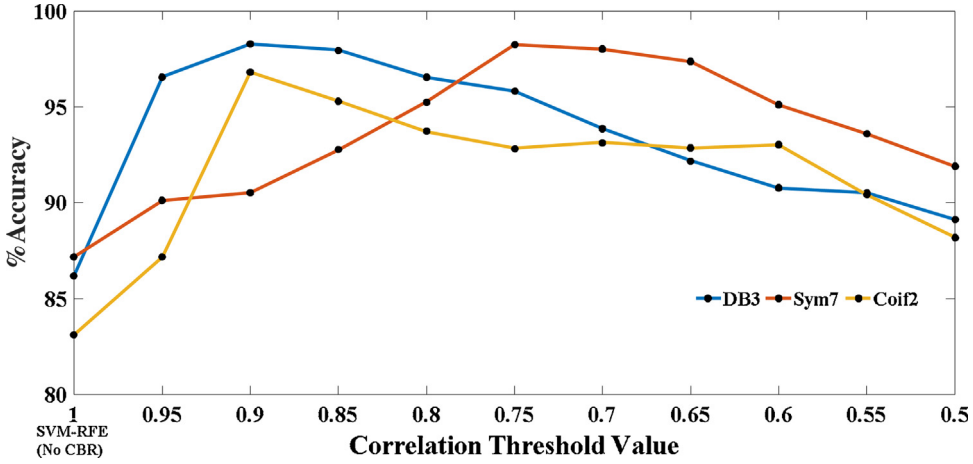

Fig. 8. Change of correct classification accuracy according to the correlation threshold value for 3rd order Daubechis, 7th order Symlet and 2nd order Coiflet mother wavelet.

dominating features for all three types of mother wavelets considered.

The classification performance for Daubechies, Symlet and Coiflet wavelets for the first 30 selected features using SVM-RFE with CBR technique, have been shown in Fig. 6. In Fig. 7 the effect of the number of selected features on the classification performance have been shown by representing the variation of classification performance parameters (sensitivity, specificity and accuracy) with the number of features from 20 to 50. It can also be clearly seen that, as expected, increase in the number of features betters the clas-

Table 2
Comparison on classification performance for different wavelet functions using SVM-RFE and SVM-RFE with CBR technique.

	SVM-RFE			SVM-RFE with CBR		
Mother Wavelet	SN (%)	SP (%)	ACC (%)	SN (%)	SP (%)	ACC (%)
Daubechies-3	91.25	80.31	86.16	97.63	100	98.28
Symlet-7	92.11	84.23	87.19	97.62	100	98.25
Coiflet-2	89.63	78.67	83.12	95.99	99.08	96.81

Table 3
Performance Comparison of the proposed method with state-of-the-art techniques.

Work	Database	No. of Images	Classification Performance (% Accuracy)
Oliveira et. al. [16]	Loyola University Chicago,YSP Dermatology Image Database, DermAtlas, DermIS, Saúde Total, Skin Cancer Guide, Dermnet – Skin Disease Atlas	408	74.36
Kasmi et. al. [17]	EDRA, Interactive Atlas of Dermoscopy	200	94
Shimizu et. al. [13]	Keio University Hospital, University of Naples and Graz, TokyoWomen'sMedical University	964	90.48
Abuzaghleh et. al. [19]	PH2 database	200	97.50
Rastgoo et. al. [12]	Vienna General Hospital	5130	Sensitivity – 98% Specificity – 70%
Barata et. al. [18]	Hospital Pedro Hispano, Matosinhos	176	Sensitivity – 96% Specificity – 80%
Garnavi et.al. [15]	–	289	91.26
Proposed Method	**International Dermoscopic Society, Dermoscopic Atlas, ISIC: challenge 2017, and PH2 database**	**4094**	**Sensitivity – 97.63% Specificity – 100% Accuracy – 98.28%**

sification performance. However, for the sake of achieving highly acceptable result with lesser number of features, first thirty features have been considered. In the feature selection stage using SVM-RFE with CBR, the selection of correlation threshold value is of prime importance. In Fig. 8 the variation of the classification accuracy with the correlation threshold value, has been shown for three selected mother wavelets. From Fig. 8 it has been observed that for the correlation threshold value ranging from 0.75 to 0.9 the highly acceptable classification accuracy has been obtained. For Daubechies wavelet family, the highest accuracy has been obtained as 98.28% for 0.9 correlation threshold value. Similarly the correlation threshold values corresponding to the highest accuracy for Symlet and Coiflet wavelet family (98.25% and 96.81% respectively) have been obtained as 0.75 and 0.9 respectively.

The results of a comparative study between SVM-RFE and SVM-RFE with CBR feature selection technique have been tabulated in Table 2. From this table it has been observed that with regard to the classification performance, the introduction of the modified correlation bias reduction technique with SVM-RFE feature selection method has outperformed the SVM-RFE method remarkably.

A comparative study of the proposed methodology with other state of the art techniques has been presented in Table 3. Oliveira et al. [16] have achieved 74.36% classification accuracy for the identification of nevus and melanoma images by introducing fractal dimension measurement technique of the lesion area, statistical color features extraction and border irregularity measurement using inflexion point and vector product descriptor method. In [17] Kasmi et al. have implemented the automatic ABCD rule to differentiate malignant melanoma from benign skin lesions and have reported a classification accuracy of 94%. The shape, color and brightness asymmetry have been measured using different mathematical operation along the smaller sub regions of the original image. The color features have been extracted by measuring the normalized Euclidean distances between each pixel of the lesion and six suspicious colors (white, black, red, light-brown, dark-brown and blue-gray) along with the presence of different structures in the lesion area. Shimizu et. al [13] have reported 90.48% accuracy for melanoma identification using layered model. In [19], Abuzaghleh et al. proposed an non-invasive real time skin lesion identification technique by extracting 2D Fast Fourier Transform, Discrete Cosine Transform and color histogram features with an accuracy of 97.5% for melanoma identification. The sensitivity of 98% has been obtained by Rastgoo et. al [12] for the differentiation of melanoma from dysplastic nevi by calculating the distance and color variance with complete local binary pattern, GLCM, histogram of oriented gradient features. The local gradient and color histogram features have been extracted for the detection of melanoma images with the 96% sensitivity and 80% specificity by Barata et. al [18]. Garnavi et. al [15] have achieved 91.26% classification accuracy for the diagnosis of melanoma, measuring different irregularity indices and statistical features at each level of the four level wavelet tree. The tabulations reveal that the proposed method achieves decent classification performance compared to the recently published methods. From Table 3 a conclusion can be drawn that the proposed methodology extracts the representative features and classify the melanoma using SVM classifier incorporating modified SVM-RFE with CBR method, with a highest accuracy level.

8. Conclusions

This paper proposes a methodical approach for the texture analysis of skin lesion. The wavelet based fractal texture analysis technique that has been introduced, is able to extract more detailed texture information that could not be obtained from the statistical texture analysis in spatial domain. A fractal based border irregularity measurement technique has been incorporated here for the quantification of the irregular nature of the various skin lesions. From the large number of features that have been extracted by means of morphological feature analysis along with texture and boarder irregularity features, the most important features have been selected introducing correlation biased reduction technique with SVM-RFE feature selection algorithm. An automatic selection of correlation threshold value has been introduced in this work. The performance of the proposed scheme is corroborated by Inter-

national Dermoscopic Society, Dermoscopic Atlas, PH2 databases, and ISIC: challenge 2017 database which are widely acceptable to the researchers. In this work for the detection of melanoma by distinguishing it from benign nevi, the best classification performance that is achieved is obtained using the first 30 selected features for 3rd order Daubechies wavelet. The corresponding sensitivity, specificity and correct classification accuracy are 97.63%, 100% and 98.28% respectively. The performance metrics of the reported scheme are quite good when compared with the state of the art schemes reported by others in this domain.

Acknowledgements

This work is supported by the Department of Electronics and IT, Govt. of India through 'Visvesvaraya PhD scheme' awarded to Jadavpur University, India. The authors would also like to acknowledgement International Dermoscopy Society and Dermoscopy Atlas, Australia and New Zealand, PH^2- A dermoscopic image database for research and benchmarking, and ISIC: challenge 2017 database for kindly allowing the authors to access the image database for this work.

References

[1] R. Marks, An overview of skin cancers: incidence and causation, Cancer 75 (January (Suppl. 2)) (1995) 607–612.
[2] J. Serup, G.B.E. Jemec, G.L. Grove, Handbook of NON-INVASIVEMETHODS and the SKIN, second edition, CRC Press, 2006.
[3] H. Pehamberger, M. Binder, A. Steiner, K. Wolff, In vivo equiluminescence microscopy: improvement of early diagnosis of melanoma, J. Invest. Dermatol. 100 (1993) 356S–362S.
[4] F. Nachbar, W. Stolz, T. Merkle, A.B. Cognetta, T. Vogt, M. Landthaler, P. Bilek, O. Braun-Falco, G. Plewig, The ABCD rule of dermatoscopy: high prospective value in the diagnosis of doubtful melanocytic skin lesions, J. Am. Acad. Dermatol. 30 (4) (1994) 551–559.
[5] S. Menzies, C. Ingvar, W. McCarthy, A sensitivity and specificity analysis of the surface microscopy features of invasive melanoma, Melanoma Res. 6 (1) (1996) 55–62.
[6] G. Argenziano, G. Fabbrocini, P. Carli, Equiluminescence microscopy for the diagnosis of doubtful melanocytic skin lesions: comparison of the ABCD rule of dermatoscopy and a new 7-point checklist based on pattern analysis, Arch. Dermatol. 134 (1998) 1563–1570.
[7] G. Argenziano, H. Soyer, S. Chimenti, R. Talamini, R. Corona, F. Sera, M. Binder, Dermoscopy of pigmented skin lesions: results of a consensus meeting via the Internet, J. Amer. Acad. Dermatol. 48 (2003) 679–693.
[8] A.R. Sadri, M. Zekri, S. Sadri, N. Gheissari, M. Mokhtari, F. Kolahdouzan, Segmentation of dermoscopy images using wavelet networks, IEEE Trans. Biomed. Engg. 60 (April (4)) (2013) 1134–1141.
[9] Z. Ma, J.M.R.S. Tavares, A novel approach to segment skin lesions in dermoscopic images based on a deformable model, IEEE J. Biomed. Health Info. 20 (March (2)) (2016) 615–623.
[10] Q. Abbas, I. Fondón, M. Rashid, Unsupervised skin lesions border detection via two-dimensional image analysis, Comp. Methods Programs Biomedic. 104 (2011) e1–e15.
[11] S. Chatterjee, D. Dey, S. Munshi, Mathematical morphology aided shape, texture and color feature extraction from skin lesion for identification of malignant melanoma, in proc, IEEE CATCON (December) (2015) 200–203.
[12] M. Rastgoo, R. Garcia, O. Morel, F. Marzani, Automatic differentiation of melanoma from dysplastic nevi, Comput. Med. Imaging Graphics 43 (2015) 44–52.
[13] K. Shimizu, H. Iyatomi, M.E. Celebi, K. Norton, M. Tanaka, Four-Class classification of skin lesions with task decomposition strategy, IEEE Trans. Biomed. Eng. 62 (January (1)) (2015) 274–283.
[14] I. Maglogiannis, K. Delibasis, Enhancing classification accuracy utilizing globules and dots features in digital dermoscopy, Comp. Method. Programs Biomed. 118 (2015) 124–133.
[15] R. Garnavi, M. Aldeen, J. Bailey, Computer-aided diagnosis of melanoma using border and wavelet-Based texture analysis, IEEE Trans. Inf. Tech. BioMed. 16 (6) (2012) 1239–1252.
[16] R.B. Oliveira, N. Marranghello, A.S. Pereira, J.M.R.S. Tavares, A computational approach for detecting pigmented skin lesions in macroscopic images, Expert Sys. Appl. 61 (2016) 53–63.
[17] R. Kasmi, K. Mokrani, Classification of malignant melanoma and benign skin lesions: implementation of automatic ABCD rule, IET Image Process. 10 (6) (2016) 448–455.
[18] C. Barata, M. Ruela, M. Francisco, T. Mendonça, J.S. Marques, Two systems for the detection of melanomas in dermoscopic images using texture and color features, IEEE Syst. J. 8 (3) (2014) 965–979.
[19] O. Abuzaghleh, B.D. Barkana, M. Faezipour, Non-invasive real-time automated skin lesion analysis system for melanoma early detection and prevention, IEEE J. Transl. Engg. Health Med. 3 (2015).
[20] S. Lahmiri, Glioma detection based on multi-fractal features of segmented brain MRI by particle swarm optimization techniques, Biomed. Signal Proces. Control. 31 (2017) 148–155.
[21] U.R. Acharya, W.L. Ng, K. Rahmat, V.K. Sudarshan, J.E.W. Koh, J.H. Tan, Y. Hagiwara, C.H. Yeong, K.H. Ng, Data mining framework for breast lesion classification in shear wave ultrasound: a hybrid feature paradigm, Biomed. Signal Proces. Control. 33 (2017) 400–410.
[22] R.M. Haralick, K. Shanmugam, I. Dinstein, Textural features for image classification, IEEE Trans. Syst. Man Cybern. 3 (November (6)) (1973) 610–621.
[23] B. Manjunath, W. Ma, Texture features for browsing and retrieval of image data, IEEE Trans. Pattern Anal. Mach. Intell. 18 (1996) 837–842.
[24] M. Pietikäinen, A. Hadid, G. Zhao, T. Ahonen, Computer Vision Using Local Binary Patterns, 2011.
[25] H. Handels, T. Rob, J. Kreuschb, H. Wolffb, S. Poppla, Feature selection for optimized skin tumor recognition using genetic algorithms, Artif. Intell. Med. 16 (199) (2016) 283–297.
[26] S. Patwardhan, A. Dhawan, P. Relue, Classification of melanoma using tree structured wavelet transforms, Comput. Methods Programs Biomed. 72 (2003) 223–239.
[27] K. Yan, D. Zhang, Feature selection and analysis on correlated gas sensor data with recursive feature estimation, Sens. Actuators B 212 (2015) 353–363.
[28] B.B. Mandelbrot, Fractals: Form, Chance and Dimensions, Freeman, San Francisco, CA, 1977.
[29] K. Falconer, FRACTAL GEOMETRY Mathematical Foundations and Applications, 2nd edition, Wiley, 2003.
[30] G.A. Edgar, Measure, Topology and Fractal Geometry, Springer, New York, USA, 1990.
[31] F. Hausdorff, Dimension und äußeresmaß, Math. Annal. 79 (1–2) (1918) 157–179.
[32] N. Sarkar, B.B. Chaudhuri, An efficient differential box-counting approach to compute fractal dimension of an image, IEEE Trans. Syst. Man Cybern. 24 (1) (1994) 115–120.
[33] J.B. Florindo, O.M. Bruno, Texture analysis by fractal descriptors over the wavelet domain using a best basis decomposition, Physica A 444 (2016) 415–427.
[34] P. Soille, Morphological Image Analysis Principles and Applications, 2nd edition, Springer, 2004.
[35] R.C. Gonzalez, R.E. Woods, Digital Image Processing, 3rd ed., Pearson, 2014.
[36] C.L. Jones, H.F. Jelinek, Wavelet packet fractal analysis of neuronal morphology, Methods 24 (August (4)) (2001) 347–358.
[37] T. Higuchi, Approach to an irregular time series on the basis of the fractal theory, Physica D 31 (1988) 277–283.
[38] M. Katz, Fractals and the analysis of waveforms, Comput. Biol. Med. 18 (3) (1988) 145–156.
[39] I. Guyon, J. Wetson, S. Barnhill, V. Vapnik, Gene selection for cancer classification using support vector machines, Mach. Learn. 46 (1–3) (2002) 389–422.
[40] V. Vapnik, The Nature of Statistical Learning Theory, Springer-Verlag, New York, 1995.
[41] M. Li, W. Chen, T. Zhang, Automatic epileptic EEG detection using DT-CWT-based non-linear features, Biomed. Signal Proces. Control 34 (2017) 114–125.
[42] L. Toloşi, T. Lengauer, Classification with correlated features: unreliability of feature ranking and solutions, Bioinformatics 27 (2011) 1986–1994.
[43] [dataset] International Dermoscopy Society, www.dermoscopy-ids.org.
[44] [dataset] Dermoscopy Atlas, www.deroscopyatlas.com.
[45] Teresa Mendonça, Pedro M. Ferreira, Jorge Marques, Andre R.S. Marcal, Jorge Rozeira, PH^2 – A dermoscopic image database for research and benchmarking, in: 35th International Conference of the IEEE Engineering in Medicine and Biology Society, July 3–7, 2013, Osaka, Japan, 2013.
[46] [dataset] The International Skin Imaging Collaboration: Melanoma Project. ISIC Archive. [Online]. Available: https://isic-archive.com.